RESEARCH PAPER

BJP | BRITISH PHARMACOLOGICAL SOCIETY

Exploring occupancy of the histamine H_3 receptor by pitolisant in humans using PET

Pablo Rusjan[1,2,9] | Pamela Sabioni[3] | Patricia Di Ciano[2,3,4,9] | Esmaeil Mansouri[1,5] | Isabelle Boileau[1,9,11] | Alexia Laveillé[6] | Marc Capet[6] | Thierry Duvauchelle[6] | Jean-Charles Schwartz[7] | Philippe Robert[7] | Bernard Le Foll[1,8,9,10,11]

[1]Research Imaging Centre, CAMH, Toronto, Canada

[2]Department of Pharmacology and Toxicology, University of Toronto, Toronto, Canada

[3]Translational Addiction Research Laboratory, CAMH, Toronto, Canada

[4]Institute for Mental Health Policy Research, CAMH, Toronto, Canada

[5]Institute of Medical Sciences, University of Toronto, Toronto, Canada

[6]Bioprojet Pharma, Paris, France

[7]Bioprojet Biotech, Paris, France

[8]Acute Care Program, CAMH, Toronto, Canada

[9]Campbell Family Mental Health Research Institute, CAMH, Toronto, Canada

[10]Department of Family and Community Medicine, University of Toronto, Toronto, Canada

[11]Division of Brain and Therapeutics, Department of Psychiatry, University of Toronto, Toronto, Canada

Correspondence
Bernard Le Foll, Research Imaging Centre, CAMH, Toronto, ON, Canada.
Email: bernard.lefoll@camh.ca

Background and Purpose: BF2.649 (pitolisant, Wakix®) is a novel histamine H_3 receptor inverse agonist/antagonist recently approved for the treatment of narcolepsy disorder. The objective of the study was to investigate in vivo occupancy of H_3 receptors by BF2.649 using PET brain imaging with the H_3 receptor antagonist radioligand [11C]GSK189254.

Experimental Approach: Six healthy adult participants were scanned with [11C]GSK189254. Participants underwent a total of two PET scans on separate days, 3 h after oral administration of placebo or after pitolisant hydrochloride (40 mg). [11C]GSK189254 regional total distribution volumes were estimated in nine brain regions of interest with the two tissue-compartment model with arterial input function using a common V_{ND} across the regions. Brain receptor occupancies were calculated with the Lassen plot.

Key Results: Pitolisant, at the dose administered, provided high (84 ± 7%; mean ± SD) occupancy of H_3 receptors. The drug was well-tolerated, and participants experienced few adverse events.

Conclusion and Implications: The administration of pitolisant (40 mg) produces a high occupancy of H_3 receptors and may be a new tool for the treatment of a variety of CNS disorders that are associated with mechanisms involving H_3 receptors.

1 | INTRODUCTION

Histamine is a biogenic amine neurotransmitter involved in many biological processes, such as the inflammatory response and regulation of gut function. There are four main histamine receptor subtypes: H_1, H_2, H_3, and H_4 (Parsons & Ganellin, 2006). The histamine H_3 receptor has been investigated as a potential target for the treatment of various CNS disorders.

The H_3 receptors are widely expressed in the human and non-human primates, with particularly high densities in the basal ganglia (Martinez-Mir et al., 1990). On histaminergic neurons, H_3 receptors are presynaptic receptors acting as autoreceptors regulating the synthesis and release of histamine (Arrang, Garbarg, & Schwartz, 1983). On non-histaminergic neurons, H_3 receptors act as heteroreceptors controlling the release of other neurotransmitters, such as acetylcholine, dopamine, and noradrenaline (Molina-Hernandez, Nunez, & Arias-Montano, 2000; Prast et al., 1999; Schlicker, Fink, Hinterthaner, & Gothert, 1989).

Due to their anatomical localization and widespread effect on other neurotransmitters mentioned above, drugs that selectively block H_3 receptors may be useful in the treatment of psychiatric and substance abuse disorders. At present, H_3 receptor inverse agonists have been primarily evaluated for the treatment of sleep disorders (narcolepsy and obstructive sleep apnoea) due to their ability to increase wakefulness (Raddatz, Tao, & Hudkins, 2010; Sander, Kottke, & Stark, 2008; Stocking & Letavic, 2008).

BF2.649 (pitolisant; Wakix®), a H_3 receptor inverse agonist, was approved in the European Union (EU) on March 31, 2016, for the treatment of narcolepsy with or without cataplexy in adults (Syed, 2016). Also, pitolisant was evaluated in Phase IIa proof of concept trials for its therapeutic potential to enhance cognition in several neuropsychiatric disorders, such as attention deficit hyperactivity disorder, schizophrenia, and dementias (Lewy bodies dementia) (Schwartz, 2011). In the typical posology in clinical trials, the oral dose of pitolisant is increased daily, based on benefit/tolerance ratio, up to 40 mg with typical observed therapeutic efficacy for daily doses between 20 and 40 mg. (Dauvilliers et al., 2019). Pitolisant plasma concentration peaked approximately 3 h after administration, and it has a plasma half-life of 10–12 h. After 5 or 6 days of repeated administrations, the steady state is achieved, and the serum level doubled (European Medicines Agency, November 22, 2018).

In preclinical radiolabelling ligand binding studies, pitolisant showed competitive antagonist effects (K_i = 0.16 nM) and inverse agonist effects (EC_{50} = 1.5 nM) at recombinant human H_3 receptors, with an intrinsic inverse agonist activity ~50% higher than the potent histamine H_3 receptor inverse agonist/antagonist ciproxifan (Ligneau et al., 2007). Similarly, pitolisant acted as a potent inhibitor (IC_{50} = 5.3 nM 5.3 ± 2.2 nM) of [^{125}]iodoproxyfan, a radiolabelled ligand at H_3 receptors isolated from the human cerebral cortex (Ligneau et al., 2007). When compared to other histamine receptor subtypes, pitolisant showed higher selectivity for H_3 receptors over human H_1 and H_4 receptors and guinea pig H_2 receptors (Ligneau et al., 2007).

Imaging techniques are useful tools to visualize receptors and their occupancy by neurotransmitters or by a selective agonist/antagonist drug. PET imaging is the gold standard to investigate brain chemistry in living humans, as it allows for the non-invasive measurement of receptor occupancy. The process of imaging requires the injection of a positron-emitting radioligand that binds to the protein of interest followed by the measurement of uptake by the PET scanner.

What is already known

- Pitolisant is a histamine H_3 receptor inverse agonist marketed as Wakix® for the treatment of narcolepsy.

What does this study add

- This study provides information on H_3 receptor occupancy obtained with pitolisant.

What is the clinical significance

- A high degree of receptor occupancy is obtained at a clinically effective dose of pitolisant.

Plisson et al. (2009) have described the radiosynthesis and preclinical evaluation of 6-[(3-cyclobutyl-2,3,4,5-tetrahydro-1H-3-benzazepin-7-yl)oxy]-N-[^{11}C]methyl-3-pyridinecarboxamide hydrochloride (^{11}C-GSK189254) as a novel PET radioligand for the H_3 receptor. GSK189254 is a highly potent, selective, and brain-penetrant H_3 receptor antagonist developed by GlaxoSmithKline, with a high affinity for both human and pig H_3 receptors (Ashworth et al., 2014; Plisson et al., 2009). Previous studies have shown that ^{11}C-GSK189254 is brain-penetrant (Ashworth et al., 2010), has appropriate kinetics for quantification (Ashworth et al., 2010), and demonstrates uptake (which can be blocked by the H_3 receptor antagonist ciproxifan) in regions of the brain that are rich in H_3 receptors (Plisson et al., 2009).

The aim of the present study was to determine the occupancy of brain H_3 receptors, 3 h after a single oral dose of 40 mg of pitolisant hydrochloride using PET with the radioligand [^{11}C]GSK189254 in healthy human volunteers.

2 | METHODS

2.1 | Human participants

Six healthy volunteers (four males and two females; aged 19–61 years) completed this study. All participants were free of current medical and psychiatric illness as assessed by self-report, physical examination, ECG, urinalysis (including drug screening), and blood tests (complete blood count and serum chemistry). All subjects provided written informed consent after all procedures were fully explained. Research Ethics Board approval was obtained at the Centre for Addiction and Mental Health. All study procedures complied with the 1975 Helsinki Declaration (5th revision, 2000).

2.2 | PET protocol

Each participant was scanned twice on separate days: The first scan occurred 3 h after an oral dose of placebo, and the second scan occurred 3 h after an oral dose (40 mg) of pitolisant hydrochloride. Due to the potential for unforeseen interactions between pitolisant and the radiotracer, a placebo was administered first to allow for the careful assessment of adverse events and to increase participant retention; thus, no randomization occurred. Although this could be considered a potential limitation of this study, participant safety was considered to be a more important determinant of the design. Following oral administration, pitolisant reaches peak plasma concentration (C_{max}) in about 3 h (European Medicines Agency, November 22, 2018). Scans were separated by an average of 33 ± 16 days. There were no differences between conditions with respect to the [11C]GSK189254 injected mass (mean ± SD, 2.8 ± 0.4 μg (placebo) vs. 2.6 ± 0.4 μg (Pitolisant)), specific activity (1,204 ± 348 mCi·μmol^{-1} vs. 1,313 ± 345 mCi·μmol^{-1} and amount injected (9.1 ± 1.6 mCi vs. 9.2 ± 1.0 mCi). In order to eliminate any potential bias caused by expectancy effects, participants were blind to the treatment condition: Participants were told that they would receive pitolisant prior to one scan and placebo prior to the other, but they would not know when they were receiving each one. To determine serum levels of pitolisant, blood was taken at 180 and 270 min after pitolisant administration, and also at baseline, prior to injection of the radiotracer.

PET was performed using a 3D High-Resolution Research Tomograph (HRRT) (CPS/Siemens, Knoxville, TN, USA), which measures radioactivity in 207 slices with an interslice distance of 1.22 mm. The detectors of the HRRT are an LSO/LYSO phoswich detector, with each crystal element measuring 2 × 2 × 10 mm^3. A transmission scan, measured using a single photon point source, ^{137}Cs ($t_{1/2}$ = 30.2 years, E_γ = 662 keV) was acquired immediately prior to the acquisition of the emission scan. This transmission scan was subsequently used to correct the emission data for the attenuation of the emission photons through the head and support. After the transmission scan, [11C]GSK189254 was injected as a rapid bolus, and emission data were acquired in list mode for 90 min following the injection. The emission list mode data were re-binned into a series of 3D sinograms. The 3D sinograms were gap-filled, scatter-corrected, and Fourier re-binned into 2D sinograms The images were reconstructed from the 2D sinograms using a 2D filtered-back projection algorithm, with a HANN filter at Nyquist cut-off frequency. The reconstructed image had 256 × 256 × 207 cubic voxels measuring 1.22 × 1.22 × 1.22 mm^3, and the resulting reconstructed resolution is close to isotropic 4.4 mm, full width at half maximum (FWHM) in-plane and 4.5 mm FWHM axially, averaged over measurements from the centre of the transaxial field of view (FOV) to 10 cm off-centre in 1.0 cm increments. Also, for frame realignment purposes, each image was reconstructed without attenuation correction using the 3D ordinary Poisson ordered subset expectation maximization (OP-OSEM3D) algorithm implemented within the hrrt_osem3d_u sw_version HRRT_U 1.3 (available from the HRRT user's group) using

three iterations and six subsets and the default PSF model (Comtat et al., 2004; Hong et al., 2007).

The images were reconstructed into 27 time frames: The first frame was of variable length being dependent on the time between the start of acquisition and the arrival of [11C]GSK189254 in the tomograph FOV. The subsequent frames were defined as 8 × 15 s, 3 × 60 s, 5 × 120 s, 5 × 300 s, and 5 × 600 s. All images were decay corrected.

A custom-fitted thermoplastic mask was made for each participant and used with a head fixation system during PET measurements to minimize head movement. Head movement in the dynamic PET acquisition was corrected using frame-by-frame realignment. Low noises, non-attenuation corrected images (created with iterative reconstruction) were used to optimize the frame-by-frame realignment process. A normalized mutual information algorithm was applied with SPM8 (Wellcome Trust Centre for Neuroimaging, London, UK) to co-register each frame to the frame from 12.25 to 17.25 min after the radioligand arrives at the FOV (frame number 12) which showed a high signal-to-noise ratio RRID:SCR_008873. Parameters from the normalized mutual information were applied to re-slice the corresponding attenuation-corrected dynamic images to generate a movement-corrected dynamic image. The frame realignment performed in this work does not correct for a potential mismatch between the emission and transmission scan or intraframe motion.

2.3 | Measurement of [11C]GSK189254 in plasma

Arterial blood samples were withdrawn continuously for the first 22 min from the radial artery cannula and counted using an automatic blood sampling system (ABSS, Model # PBS-101 from Veenstra Instruments, Joure, Netherlands). Polytetrafluoroethylene tubing was used to minimize tube adhesion of [11C]GSK189254. The rate of the blood pump was 350 ml·h^{-1} the first 7.25 min and then slowed to 150 ml·h^{-1}. Also, manual samples were taken close to the wrist of the subject at t = 3.5, 7, 12, 15, 20, 30, 45, 60, 80 min at volumes between 5 and 10 ml. The ABSS line was rinsed with a saline solution after the manual samples were acquired at 12, 15, and 20 min (Lammertsma et al., 1991). Radioactivity in each manual blood sample was counted using a 2480 WIZARD (Perkin Elmer, Waltham, MA) gamma counter cross-calibrated with the PET. Concentration in the samples at t = 12, 15, and 20 min was used to calibrate the ABSS. A blood time-activity curve (TAC) for 90 min was created from merging the ABSS output data, excluding the rinse periods, with the manual sample measurements. The blood samples were centrifuged (1,500× g, 5 min) and a plasma aliquot counted. The blood-to-plasma ratios determined from the manual samples showed little change along the time without a systematic pattern across subjects; therefore, it was model as a constant. The value of the constant was calculated individually for each scan as the average of the measurements for that scan. Plasma TAC was derived from dividing the blood TAC by the ratio of blood to plasma.

The remaining volume of each plasma sample was used to determine the fraction of parent radioligand in plasma $P(t)$ using a solid-phase cartridge method. For five subjects $P(t)$ was fitted with a Hill-type function: $P(t) = R_0 - at^b/(t^b+c^b)$ (being R_0 the radiochemistry purity), but for one subject in baseline and blocked condition the pattern of $P(t)$ was different, and it was fitted with a bi-exponential. On that subject, the radiochemistry purity was lower than in the other scans (95.1% in the placebo and 96.7% in blocked condition). For the rest of the scans, the radiochemistry purity was ≥99% except for a case in which it was 97.8%. A metabolite-corrected plasma curve to be used as the input function for the kinetic analysis was generated multiplying the plasma TAC by $P(t)$.

Five minutes before each scan injection, an arterial plasma sample was collected and frozen. All collected samples were unfrozen on the same day, and [^{11}C]GSK189254 free fraction in plasma (fp) was determined by the ultrafiltration method (Gandelman, Baldwin, Zoghbi, Zea-Ponce, & Innis, 1994).

2.4 | Delay and dispersion

Delay and dispersion were estimated using the head curve (true events per second in the FOV) up to 55 s after the activity starting in the FOV as described previously (Rusjan et al., 2014). Briefly, a 1TCM model was fitted to the head curve using the dispersion-corrected ABSS signal as input function. The dispersion was modelled as a mono-exponential convolution, and the deconvolution was performed iteratively. Dispersion is including as a variable during the fitting of the delay. Delay and dispersion are assumed to be the same value for all the regions of interest (ROIs).

2.5 | Magnetic resonance image and regions of interest delineation

For the anatomical delineation of ROIs, a brain magnetic resonance image (MRI) was acquired for each subject. The MR scans were performed on a Discovery™ MR750 3.0T GE scanner (Milwaukee, WI, USA) equipped with an 8-channel headcoil. Two-dimensional axial proton density (PD) images were acquired as follows: fast spin-echo imaging (FSE), echo time (TE)/repetition time (TR)/echo train length = MinFull/6 s/8, receiver BW ± 15.63 kHz, FOV = 22 cm, 256 × 256 sampling matrix, slice thickness = 2 mm and a parallel imaging acceleration factor of 2. ROIs for the cerebellar cortex, head of the caudate (hereafter referred to as caudate), putamen, thalamus and temporal, prefrontal, occipital, anterior cingulate, and insula cortices were automatically generated based on individual PD-MRIs using in-house imaging pipeline, ROMI (Rusjan et al., 2006). This arbitrary selection of ROIs includes big ROIs (i.e., less noise in the TACs) and presents a spread of H$_3$ receptor concentration in order to apply the Lassen Plot (see below). ROMI utilizes computer vision techniques based on the probabilities of grey matter to fit a standard template of ROIs to an individual high-resolution MRI scan. The individual MRI images are

then registered to a summed PET image so that the individualized ROIs are transformed into the PET image space and regional TAC extracted. Co-registration was done using SPM2 (Wellcome Trust Centre for Neuroimaging, London, UK), optimizing a measure of normalized mutual information (Studholme, Hill, & Hawkes, 1999).

2.6 | Data and statistical analysis

2.6.1 | Kinetic analysis

Regional total distribution volume (V_T) was estimated with a two tissue-compartment model (2TCM). All the regions were fitted simultaneously using a common value for the distribution volume of the non-displaceable compartment (V_{ND}) The vascular fraction was fixed to 5% in all the regions (Ito et al., 2004). The kinetic model was applied using PMOD 3.4 (PMOD Technologies, Zurich, Switzerland). The default restrictions of PMOD were used forcing the rate constants to be non-negative. Data points were weighted with $w_i = \Delta t_i/(e^{\lambda t_i}C_i)$ where C_i is the activity at the frame at t_i of length Δt_i and $\lambda = \ln(2)/20.39$ min is the decay constant of ^{11}C. Brain occupancies (Occ) were calculated using the Lassen plot: $V_T^{placebo} - V_T^{block} = Occ\left(V_T^{placebo} - V_{ND}\right)$ (Cunningham, Rabiner, Slifstein, Laruelle, & Gunn, 2010; Lassen et al., 1995). The set of ROIs analysed shows a reasonable spread of V_T values.

2.6.2 | Analysis of serum levels of pitolisant

Blood samples were collected without any anticoagulant and serum samples, obtained by centrifugation at 4°C at 1,500× g for 10 min, were stored frozen at −80°C until the determination of serum concentrations. Serum was extracted along with an internal standard by solid-phase extraction using Oasis$^®$ HLB microelution cartridges (Waters) using a generic method. Serum concentrations of pitolisant were measured using a validated analytical method according to the European Medicines Agency (EMA) guidance in a Good Laboratory Practices compliant laboratory. In particular, the standard curve we used for measuring serum levels of pitolisant complied with EMA guidance on bioanalytical method validation.

The method was an electrospray LC-tandem MS (LC–MS/MS) analysis with a Waters Xevo TQMS quadrupole mass spectrometer equipped with an Acquity$^®$ ultra-HPLC (UHPLC) pump (Waters, France). For chromatographic separation, a Acquity UPLC$^®$ BEH C18 column (50 × 2.1 mm ID, particle size 1.7 μm; Waters, France) was used with a mobile phase consisting of acetonitrile/water (10/90, v/v) containing 0.1% formic acid (A) and acetonitrile containing 0.1% formic acid (B). The flow rate was 0.8 ml·min^{-1}, and the gradient programme was as follows: (min, B%) = (0, 0), (0.2, 5), (4.2, 33), (5.0, 100), (5.5, 0) The column temperature was set at 50°C. Mass spectra were acquired in the positive ionization mode by multiple reactions monitoring (MRM). The capillary voltage was set at 1.1 kV, and the source and desolvation temperatures were 150 and 600°C, respectively.

Cone and desolvation gas (N_2) flows were set at 50 and 1,200 $L·h^{-1}$, respectively. Argon was used as the collision gas at a pressure of 3.6 × 10−3 mbar. The MRM transition, cone voltage, and collision energy were set to m/z 296.2 → 98.2, 35 V, 30 V for pitolisant. The standard curve ranged from 0.1 to 100 $ng·ml^{-1}$. A proprietary compound was used as an internal standard.

2.6.3 | Statistical analysis

The paired sample *t*-test was used when comparing magnitudes between the placebo and the pitolisant scans or between methods of analysis. The analyses were two-tailed, except when it is specified, and we considered results to be significant at $P ≤ 0.05$. The data and statistical analysis comply with the recommendations of the *British Journal of Pharmacology* on experimental design and analysis in pharmacology.

2.6.4 | Power analysis

The present study was a pilot investigation, and thus, a sample size of six was considered appropriate.

2.7 | Materials

BF2.649, pitolisant (1-piperidine, hydrochloride) was obtained from Bioprojet Pharma. [11C]GSK189254 was synthesized at the Centre for Addiction and Mental Health as previously described in Ashworth et al (Ashworth et al., 2010).

2.8 | Nomenclature of targets and ligands

Key protein targets and ligands in this article are hyperlinked to corresponding entries in http://www.guidetopharmacology.org, the common portal for data from the IUPHAR/BPS Guide to PHARMA-COLOGY (Harding et al., 2018), and are permanently archived in the Concise Guide to PHARMACOLOGY 2019/20 (Alexander et al., 2019).

3 | RESULTS

3.1 | Adverse events

Adverse events were assessed by asking the participants about any effects of the drugs and were also measured using the UKU side effects rating scale. The UKU side effects rating scale reports adverse events for the 3 days prior to drug intake as well as those occurring after. Adverse events related to the drug or placebo were reported by one out of the six participants. This participant reported increased duration of sleep that was possibly related to the single dose of 40 mg

of pitolisant. This participant also reported dystonia and orthostatic dizziness that were possibly related to administration of the placebo.

Two out of six participants reported adverse events that occurred in the 3 days prior to drug intake and were thus improbably related to the drug, given that they occurred in the 3 days (UKU) leading to the drug intake day. The adverse events reported were increased sexual desire (1), sleepiness (1), rigidity (1), increased sleep (1), and failing memory (1).

3.2 | Blood analysis

3.2.1 | Serum levels of pitolisant

For one participant, the blood sample to determine the serum levels of pitolisant was missing at 180 min; therefore, the following analysis was done with $n = 5$. Serum levels of pitolisant at ~270 min (mean ± *SD*, 25.1 ± 7.9 $ng·ml^{-1}$) were on average ~50% (range −30% to 137%) higher than ~180 min (16.6 ± 9.2 $ng·ml^{-1}$). However, this difference was not statistically significant.

3.2.2 | [11C]GSK189254 free fraction

All the arterial samples collected were unfrozen on the same day, and *f*p was determined by the ultrafiltration method. *f*p increased significantly from 28% ± 4% (mean ± *SD*) in placebo condition to 31% ± 4% after pitolisant (one-tailed, paired *t*-test). However, the *f*p difference decreased and lost significance when a correction for an order of sample analysis, which affected the data was applied (i.e., *f*p correlated with order of sample analysis, $r = 0.6$, in a batch of 32 samples analysed). The analysis in the rest of this work ignores *f*p.

3.2.3 | Input function

The radioligand [11C]GSK189254 was metabolized more rapidly when given with placebo than after pitolisant. On average, along the time-samples, there were 3.3 ± 3.4% points more parent compound in plasma in the blocked condition (Figure 1). As well, the input function presented an AUC at 90 min 12% ± 10% lower in the placebo condition than in the blocked condition. This is consistent with more radioligand available in the plasma due to a lower amount of H_3 receptors available for binding.
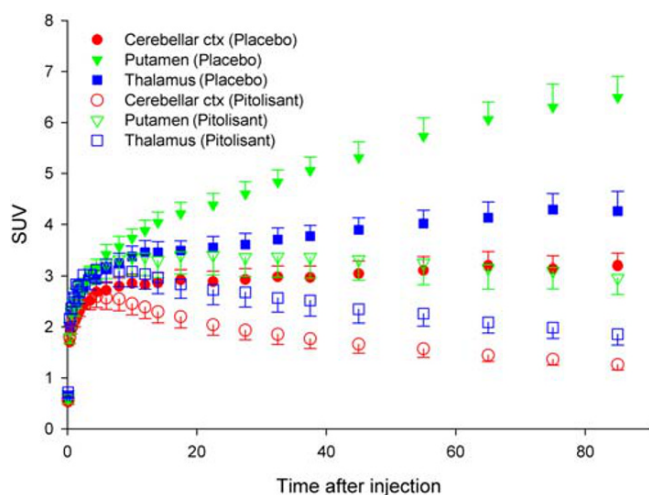
3.2.4 | Image quantification

TACs showed a dramatic change after the pitolisant (Figure 2). TACs did not show washout at any time in the baseline. Uptake levels and rank orders were consistent with those previously reported (Gallezot et al., 2017). With few exceptions, in the putamen, TACs showed a peak followed by a washout after pitolisant (40 mg). The 2TCM fitted
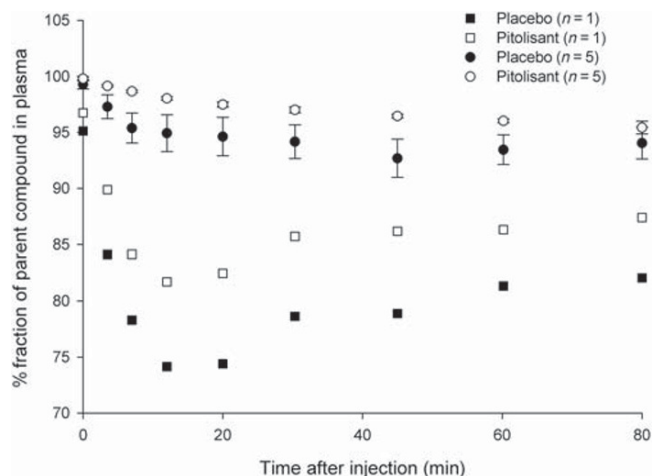
FIGURE 1 Eighty minutes after the radioligand injection, most of the radioactivity in plasma still corresponded to parent compound. The metabolism of the radioligand was slower following pitolisant than after placebo. While for 5 subjects (shown in circles; means ± SD), the observations followed the typical hill function shape, for one of the participants (shown in square symbols), metabolism showed a different pattern. For this subject, the radioligand had lower radiochemistry purity in both scans

TABLE 1 Comparison of the total volume of distribution (V_T) of [^{11}C]GSK189254 after placebo and after pitolisant

	Placebo (n = 6)		Pitolisant (n = 6)	
	M	**SD**	**M**	**SD**
Cerebellar cortex	13.1	1.6	5.0	0.9
Occipital cortex	13.4	2.5	5.3	0.9
Temporal cortex	16.3	2.2	5.8	1.2
Thalamus	18.8	2.0	6.7	1.4
Prefrontal cortex	19.1	1.1	6.2	1.3
Insula cortex	24.0	4.4	6.9	1.6
Anterior cingulate cortex	25.9	3.4	7.4	1.7
Caudate	43.9	9.3	9.8	2.8
Putamen	46.9	9.4	10.6	3.2

Note. [^{11}C]GSK189254 total volume of distribution (V_T) in different regions of interest following placebo or a single dose of 40 mg of pitolisant (n = 6). Values of V_T after pitolisant were significantly different from values after placebo ($P < 0.05$) in all the regions. V_T is expressed in ml·cm^{-3}.
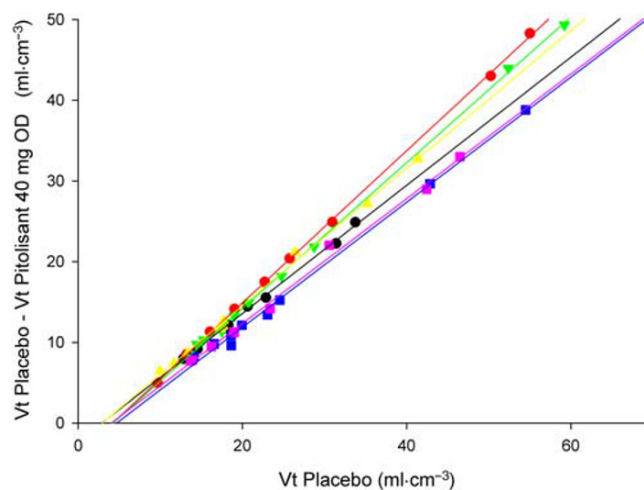

FIGURE 2 Time activity curves (TACs) for the putamen, thalamus and cerebellar cortex which are known to have high, medium and low concentration of H$_3$ receptors respectively. Following pitolisant, the TACs showed a dramatic change of shape, consistent with fewer receptors available for binding. While after placebo, the TACs did not start to decay within the scan period of 90 min, after pitolisant they showed a peak followed by a washout of activity. TACs were normalized by activity injected and weight of the subject and are expressed in standard uptake values (SUV). The data shown are means ± SD; n = 6

FIGURE 3 The Lassen plots (difference of the total distribution volume (Vt) between scans and the Vt after placebo) presented a good linearity. Each colour represents a subject and each symbol represents the data for an anatomical brain region. The slope of the lines in the Lassen plot provides the brain occupancy (one per subject), at peak plasma concentration (3 hours) following an oral dose (OD) of 40 mg of pitolisant

the TACs. Total distribution volume (V_T) was estimated sharing V_{ND} across ROI and fitting simultaneously all the ROIs (Table 1). Each participant's brain occupancy was estimated with the Lassen plot (Cunningham et al., 2010; Lassen et al., 1995). Lassen plots with the subset of ROIs selected presented excellent linearity (Figure 3). The

pitolisant (40 mg OD) occupancy was 84 ± 7% (mean ± *SD*), ranging between 77% and 94%.

4 | DISCUSSION

The purpose of the present study was to determine the occupancy of H$_3$ receptors by BF2.649 (pitolisant) at a plasma concentration consistent with that producing a therapeutic effect. The data from six participants demonstrated H$_3$ receptor occupancy of 84% ± 7% (mean ± *SD*), 3 h after an oral dose of 40 mg pitolisant hydrochloride. The

pitolisant serum concentration was 16.6 ± 9.2 ng·ml^{-1} and 25.1 ± 7.9 ng·ml^{-1} at the beginning and the end of the scan, respectively, which has been shown previously to be the serum peak time. Occupancy of 84% demonstrates significant potential for BF2.649 (pitolisant) to be an efficient pharmacological agent targeting the H$_3$ receptors. This is supported further by the fact that the dose of pitolisant used in the present study was low, and it was well-tolerated. One out of the six participants reported only one adverse effect possibly related to the drug intake, which was increased sleep. This suggests that pitolisant has a safe drug profile and warrants further testing in humans for psychiatric and behavioural disorders. This interpretation of the results assumes that the brain free concentration is in equilibrium with the free plasma concentration at all times and that the repeated dose would not produce a significant up-regulation or down-regulation of the system. Further investigations are warranted.

The use of [^{11}C]GSK189254 PET to quantify the availability of H$_3$ receptors has many challenges that should be mentioned. Firstly, the TAC at baseline condition does not show a peak, which makes the quantification of noise TAC, usually associated with small ROIs, challenging. While in earlier work using [^{11}C]GSK189254 in humans (Ashworth et al., 2010; Ashworth et al., 2014; Gallezot et al., 2017), V_{ND} and k_4 were simultaneously fitted for all the ROIs; in the results presented here, only V_{ND} was constrained. Constraining k_4 did not change the final occupancy ($84\% \pm 7\%$). The set of ROIs was chosen to be large areas with widespread V_T values, which is optimum for the application of the Lassen plot. The caudate and putamen have V_T values twofold or threefold that of the other regions, which eventually would drive the Lassen plot. However, the occupancy calculated after excluding these regions did not change ($83 \pm 10\%$). We tried other approaches to estimate V_T, which yielded the same range of occupancies for pitolisant. However, they showed points in the Lassen plot misaligned that if not removed could drive the linear correlation (e.g., when the smaller ROIs were fitted with an unconstrained 2TCM in some cases $k_4 \rightarrow 0$ giving very high V_T values).

A second challenge was that, although the rank order of the V_T values in this work are consistent with known H$_3$ receptor densities post-mortem and are very close to those published by Gallezot et al. (2017), they were, however, about double those in Ashworth et al. (2010). We have not observed the problems of dispersion mentioned in Ashworth et al. (2010), and K_1 values were in a reasonable range, consistent with the high uptake of the radioligand in the brain. We did not find the need to fit simultaneously k_4 between ROIs. Thus, the dispersion of the radioligand does not look to be greater than fluoride, which makes sense because of the moderate lipophilicity of the radioligand.

A third challenge is that, because [^{11}C]GSK189254 has a high affinity for H$_3$ receptors, radioligand mass effects could confound the quantification. In humans, same day test–retest studies showed lower V_T values in the second scan (~30% in Ashworth et al., 2010, and ~20% in Gallezot et al., 2017), and in the baboon, the dependence of V_T on mass injected was carefully determined (Logan et al., 2012). While pitolisant scans were acquired at least 2 weeks after

the placebo, and V_T values of the second scan therefore are unlikely to be affected by carryover of "cold radioligand" from the first scan, tracer mass-dose effects could still underestimate V_T values in both scans, eventually differently, and therefore affect the occupancy estimation. As a part of a larger study, we have a database of 22 [^{11}C]GSK189254 placebo scans, and we could not find any dependence of the V_T (e.g., temporal cortex) with the mass injected (1.34–3.28 µg) even after normalizing by participant weight (0.023–0.048 µg·kg^{-1}). However, a larger range of mass injected is probably needed to visualize a non-tracer mass effect. A non-tracer carryover effect correction for [^{11}C]GSK189254 has been proposed (Gallezot et al., 2017). It is based on assumptions that are difficult to verify and requires the f_p values, which we could not measure reliably. Assuming f_p values were acceptable, and using the "apparent" occupancy estimated above, the plasma concentration of [^{11}C]GSK189254 and an indirect measurement of $K_D = 9.5$ pM (Gallezot et al., 2017), the corrected "true" occupancy increases 6% points to $90 \pm 5\%$.

Ignoring the mismatch between the emission and transmission scan during the motion correction and the intraframe motion could produce error of quantification for large motions. In this work, only one scan in the blocked showed an excessive motion, all the other 11 scans presented motion below the resolution of the scanner. The brain occupancy of the subject with the large motion, after frame realignment, was 85%; therefore, including or excluding it does not change the result.

In summary, the results of this study showed that, in healthy subjects, a therapeutic dose of pitolisant occupied a large fraction of histamine H$_3$ receptors.

AUTHOR CONTRIBUTIONS
I.B., B.L.F., J.C.S., A.L., M.C., T.D., J.C.S., and P.R. participated in research design. P.S., P.D.C., E.M., and B.L.F. conducted the experiments. P.M.R. contributed with analysis tools. P.M.R., M.E., P.D.C., and P.R. performed data analysis. P.M.R., P.S., P.D.C., P.R., and B.L.F. wrote or contributed to the writing of the manuscript.

CONFLICT OF INTEREST
P.R., P.S., P.D.C., E.M., and I.B. declare no conflict of interest. A.L., M.C., and P.R. are employees of Bioprojet Biotech. Dr. Le Foll has obtained funding from Pfizer (GRAND Awards, including salary support) for investigator-initiated projects. Dr. Le Foll has/will receive some in-kind donation of a cannabis product from Canopy and Aurora and medication donation from Pfizer and Bioprojet and was provided a coil for TMS study from Brainsway. Dr. Le Foll has/will perform research with industry funding obtained from Canopy (through research grants handled by CAMH or University of Toronto, Aphria

DECLARATION OF TRANSPARENCY AND SCIENTIFIC RIGOUR

This Declaration acknowledges that this paper adheres to the principles for transparent reporting and scientific rigour of preclinical research as stated in the BJP guidelines for Design & Analysis, and as recommended by funding agencies, publishers and other organisations engaged with supporting research.

FUNDING INFORMATION

ORCID

Pamela Sabioni https://orcid.org/0000-0003-2687-9757
Esmaeil Mansouri https://orcid.org/0000-0002-8906-1314

REFERENCES

Alexander, S. P. H., Christopoulos, A., Davenport, A. P., Kelly, E., Mathie, A., Peters, J. A., ... Davies, J. A. (2019). The concise guide to pharmacology 2019/20: G protein-coupled receptors. *British Journal of Pharmacology*, *176*, S21–s141.

Arrang, J. M., Garbarg, M., & Schwartz, J. C. (1983). Auto-inhibition of brain histamine release mediated by a novel class (H3) of histamine receptor. *Nature*, *302*, 832–837. https://doi.org/10.1038/302832a0

Ashworth, S., Berges, A., Rabiner, E. A., Wilson, A. A., Comley, R. A., Lai, R. Y., ... Cunningham, V. J. (2014). Unexpectedly high affinity of a novel histamine H(3) receptor antagonist, GSK239512, in vivo in human brain, determined using PET. *British Journal of Pharmacology*, *171*, 1241–1249. https://doi.org/10.1111/bph.12505

Ashworth, S., Rabiner, E. A., Gunn, R. N., Plisson, C., Wilson, A. A., Comley, R. A., ... Cunningham, V. J. (2010). Evaluation of 11C-GSK189254 as a novel radioligand for the H3 receptor in humans using PET. *Journal of Nuclear Medicine: Official Publication, Society of Nuclear Medicine*, *51*, 1021–1029. https://doi.org/10.2967/jnumed.109.071753

Comtat C, Bataille F, Michel C, Jones JP, Sibomana M, Janeiro L, Trebossen R (2004). OSEM-3D reconstruction strategies for the ECAT HRRT. In Nuclear Science Symposium Conference Record. IEEE, pp 3492-3496.

Cunningham, V. J., Rabiner, E. A., Slifstein, M., Laruelle, M., & Gunn, R. N. (2010). Measuring drug occupancy in the absence of a reference region: The Lassen plot re-visited. *Journal of Cerebral Blood Flow and Metabolism*, *30*, 46–50. https://doi.org/10.1038/jcbfm.2009.190

Dauvilliers, Y., Arnulf, I., Szakacs, Z., Leu-Semenescu, S., Lecomte, I., Scart-Gres, C., ... Szakacs, Z. (2019). Long-term use of pitolisant to treat patients with narcolepsy: Harmony III Study. *Sleep*, *42*(11), zsz174. https://doi.org/10.1093/sleep/zsz174

European Medicines Agency. n.d. *22/11/2018 Wakix - EMEA/H/C/002616 - IB/0016* [Online] Available from https://www.ema.europa.eu/documents/product-information/wakix-epar-product-information_en.pdf. [Accessed: 22/05/2019].

Gallezot, J. D., Planeta, B., Nabulsi, N., Palumbo, D., Li, X., Liu, J., ... Carson, R. E. (2017). Determination of receptor occupancy in the presence of mass dose: [(11)C]GSK189254 PET imaging of histamine H3 receptor occupancy by PF-03654746. *Journal of Cerebral Blood Flow and Metabolism: Official Journal of the International Society of Cerebral Blood Flow and Metabolism*, *37*, 1095–1107. https://doi.org/10.1177/0271678X16650697

Gandelman, M. S., Baldwin, R. M., Zoghbi, S. S., Zea-Ponce, Y., & Innis, R. B. (1994). Evaluation of ultrafiltration for the free-fraction determination of single photon emission computed tomography (SPECT) radiotracers: β-CIT, IBF, and iomazenil. *Journal of Pharmaceutical Sciences*, *83*, 1014–1019. https://doi.org/10.1002/jps.2600830718

Harding, S. D., Sharman, J. L., Faccenda, E., Southan, C., Pawson, A. J., Ireland, S., ... NC-IUPHAR. (2018). The IUPHAR/BPS guide to pharmacology in 2018: Updates and expansion to encompass the new guide to immunopharmacology. *Nucleic Acid Research*, *46*, D1091–D1106. https://doi.org/10.1093/nar/gkx1121

Hong, I. K., Chung, S. T., Kim, H. K., Kim, Y. B., Son, Y. D., & Cho, Z. H. (2007). Ultra fast symmetry and SIMD-based projection-backprojection (SSP) algorithm for 3-D PET image reconstruction. *IEEE Transactions on Medical Imaging*, *26*, 789–803. https://doi.org/10.1109/tmi.2007.892644

Ito, H., Kanno, I., Kato, C., Sasaki, T., Ishii, K., Ouchi, Y., ... Senda, M. (2004). Database of normal human cerebral blood flow, cerebral blood volume, cerebral oxygen extraction fraction and cerebral metabolic rate of oxygen measured by positron emission tomography with ^{15}O-labelled carbon dioxide or water, carbon monoxide and oxygen: A multicentre study in Japan. *European Journal of Nuclear Medicine and Molecular Imaging*, *31*, 635–643. https://doi.org/10.1007/s00259-003-1430-8

Lammertsma, A. A., Bench, C. J., Price, G. W., Cremer, J. E., Luthra, S. K., Turton, D., ... Frackowiak, R. S. (1991). Measurement of cerebral monoamine oxidase B activity using L-[11C]deprenyl and dynamic positron emission tomography. *Journal of Cerebral Blood Flow and Metabolism*, *11*, 545–556. https://doi.org/10.1038/jcbfm.1991.103

Lassen, N. A., Bartenstein, P. A., Lammertsma, A. A., Prevett, M. C., Turton, D. R., Luthra, S. K., ... Andersen, J. V. (1995). Benzodiazepine receptor quantification in vivo in humans using [11C]flumazenil and PET: Application of the steady-state principle. *Journal of Cerebral Blood Flow and Metabolism*, *15*, 152–165. https://doi.org/10.1038/jcbfm.1995.17

Ligneau, X., Perrin, D., Landais, L., Camelin, J. C., Calmels, T. P., Berrebi-Bertrand, I., ... Bertaina-Anglade, V. (2007). BF2.649 [1-{3-[3-(4-Chlorophenyl)propoxy]propyl}piperidine, hydrochloride], a nonimidazole inverse agonist/antagonist at the human histamine H3 receptor: Preclinical pharmacology. *The Journal of Pharmacology and Experimental Therapeutics*, *320*, 365–375. https://doi.org/10.1124/jpet.106.111039

Logan, J., Carruthers, N. I., Letavic, M. A., Sands, S., Jiang, X., Shea, C., ... Fowler, J. S. (2012). Blockade of the brain histamine H3 receptor by JNJ-39220675: Preclinical PET studies with [(1)(1)C]GSK189254 in anesthetized baboon. *Psychopharmacology*, *223*, 447–455. https://doi.org/10.1007/s00213-012-2733-x

Martinez-Mir, M. I., Pollard, H., Moreau, J., Arrang, J. M., Ruat, M., Traiffort, E., ... Palacios, J. M. (1990). Three histamine receptors (H1, H2 and H3) visualized in the brain of human and non-human primates. *Brain Research*, *526*, 322–327. https://doi.org/10.1016/0006-8993(90)91240-H

Molina-Hernandez, A., Nunez, A., & Arias-Montano, J. A. (2000). Histamine H3-receptor activation inhibits dopamine synthesis in rat striatum. *Neuroreport*, *11*, 163–166. https://doi.org/10.1097/00001756-200001170-00032

Parsons, M. E., & Ganellin, C. R. (2006). Histamine and its receptors. *British Journal of Pharmacology*, *147*(Suppl 1), S127–S135.

Plisson, C., Gunn, R. N., Cunningham, V. J., Bender, D., Salinas, C. A., Medhurst, A. D., ... Gee, A. D. (2009). 11C-GSK189254: A selective radioligand for in vivo central nervous system imaging of histamine H3

receptors by PET. *Journal of Nuclear Medicine*, *50*, 2064–2072. https://doi.org/10.2967/jnumed.109.062919

Prast, H., Tran, M. H., Fischer, H., Kraus, M., Lamberti, C., Grass, K., & Philippu, A. (1999). Histaminergic neurons modulate acetylcholine release in the ventral striatum: Role of H3 histamine receptors. *Naunyn-Schmiedeberg's Archives of Pharmacology*, *360*, 558–564. https://doi.org/10.1007/s002109900097

Raddatz, R., Tao, M., & Hudkins, R. L. (2010). Histamine H3 antagonists for treatment of cognitive deficits in CNS diseases. *Current Topics in Medicinal Chemistry*, *10*, 153–169. https://doi.org/10.2174/156802610790411027

Rusjan, P., Mamo, D., Ginovart, N., Hussey, D., Vitcu, I., Yasuno, F., … Kapur, S. (2006). An automated method for the extraction of regional data from PET images. *Psychiatry Research*, *147*, 79–89. https://doi.org/10.1016/j.pscychresns.2006.01.011

Rusjan, P. M., Wilson, A. A., Miler, L., Fan, I., Mizrahi, R., Houle, S., … Meyer, J. H. (2014). Kinetic modeling of the monoamine oxidase B radioligand [(1)(1)C]SL25.1188 in human brain with high-resolution positron emission tomography. *Journal of Cerebral Blood Flow and Metabolism*, *34*, 883–889. https://doi.org/10.1038/jcbfm.2014.34

Sander, K., Kottke, T., & Stark, H. (2008). Histamine H3 receptor antagonists go to clinics. *Biological & Pharmaceutical Bulletin*, *31*, 2163–2181. https://doi.org/10.1248/bpb.31.2163

Schlicker, E., Fink, K., Hinterthaner, M., & Gothert, M. (1989). Inhibition of noradrenaline release in the rat brain cortex via presynaptic H3 receptors. *Naunyn-Schmiedeberg's Archives of Pharmacology*, *340*, 633–638. https://doi.org/10.1007/bf00717738

Schwartz, J. C. (2011). The histamine H3 receptor: From discovery to clinical trials with pitolisant. *British Journal of Pharmacology*, *163*, 713–721. https://doi.org/10.1111/j.1476-5381.2011.01286.x

Stocking, E. M., & Letavic, M. A. (2008). Histamine H3 antagonists as wake-promoting and pro-cognitive agents. *Current Topics in Medicinal Chemistry*, *8*, 988–1002.

Studholme, C., Hill, D. L. G., & Hawkes, D. J. (1999). An overlap invariant entropy measure of 3D medical image alignment. *Pattern Recognition*, *32*, 71–86.

Syed, Y. Y. (2016). Pitolisant: First Global Approval. *Drugs*, *76*, 1313–1318.